

1 **Measurement Report: Effects of anthropogenic emissions and**  
2 **environmental factors on biogenic secondary organic aerosol**  
3 **(BSOA) formation in a coastal city of Southeastern China**

4

5 Youwei Hong<sup>a,b,c,d\*</sup>, Xinbei Xu<sup>a,b,c</sup>, Dan Liao<sup>e</sup>, Taotao Liu<sup>a,b,c</sup>, Xiaoting Ji<sup>a,b,c</sup>, Ke Xu<sup>a,b,d</sup>,  
6 Chunyang Liao<sup>f</sup>, Ting Wang<sup>g</sup>, Chunshui Lin<sup>g</sup>, Jinsheng Chen<sup>a,b,c\*</sup>

7

8 <sup>a</sup>Center for Excellence in Regional Atmospheric Environment, Institute of Urban Environment,  
9 Chinese Academy of Sciences, Xiamen, 361021, China

10 <sup>b</sup>Key Lab of Urban Environment and Health, Institute of Urban Environment, Chinese Academy  
11 of Sciences, Xiamen, 361021, China

12 <sup>c</sup>University of Chinese Academy of Sciences, Beijing, 100049, China

13 <sup>d</sup>School of Life Sciences, Hebei University, Baoding, 071000, China

14 <sup>e</sup>College of Environment and Public Health, Xiamen Huaxia University, Xiamen 361024, China

15 <sup>f</sup>State Key Laboratory of Environmental Chemistry and Ecotoxicology, Research Center for Eco-  
16 Environmental Sciences, Chinese Academy of Sciences, Beijing 100085, China

17 <sup>g</sup> Institute of Earth Environment, Chinese Academy of Sciences, Xi'an, 710061, China

18

19 \*Corresponding author E-mail: Jinsheng Chen ([jschen@iue.ac.cn](mailto:jschen@iue.ac.cn)); Youwei Hong  
20 ([ywhong@iue.ac.cn](mailto:ywhong@iue.ac.cn))

21

22

23

24

25

26

27

28

29

30

31

32

33

34 **Abstract:**

35 To better understand the formation of biogenic secondary organic aerosol (BSOA),  
36 aerosol samples with a 4 h time resolution were collected during summer and  
37 wintertime in the southeast of China, along with on-line measurements of trace gases,  
38 aerosol chemical compositions, and meteorological parameters. The samples were  
39 analyzed by gas chromatography-mass spectrometry for PM<sub>2.5</sub>-bound SOA tracers,  
40 including isoprene (SOA<sub>I</sub>),  $\alpha/\beta$ -pinene (SOA<sub>M</sub>),  $\beta$ -caryophyllene (SOA<sub>C</sub>), and toluene  
41 (ASOA). The average concentrations of total SOA tracers in winter and summer were  
42 38.8 and 111.9 ng m<sup>-3</sup>, respectively, with the predominance of SOA<sub>M</sub> (70.1% and  
43 45.8%), followed by SOA<sub>I</sub> (14.0% and 45.6%), ASOA (11.0% and 6.2%) and SOA<sub>C</sub>  
44 (4.9% and 2.3%). Compared to those in winter, the majority of BSOA tracers in summer  
45 showed significant positive correlations with Ox (O<sub>3</sub>+NO<sub>2</sub>) ( $r = 0.443 \sim 0.808$ ), HONO  
46 ( $r = 0.299 \sim 0.601$ ), ultraviolet (UV) ( $r = 0.382 \sim 0.588$ ) and temperature (T) ( $r =$   
47  $0.529 \sim 0.852$ ), indicating the influence of photochemical oxidation under relatively  
48 clean conditions. However, in winter, BSOA tracers were significantly correlated with  
49 PM<sub>2.5</sub> ( $r = 0.407 \sim 0.867$ ), NO<sub>3</sub><sup>-</sup> ( $r = 0.416 \sim 0.884$ ), SO<sub>4</sub><sup>2-</sup> ( $r = 0.419 \sim 0.813$ ), and NH<sub>3</sub>  
50 ( $r = 0.440 \sim 0.757$ ), attributed to the contributions of anthropogenic emissions. Major  
51 BSOA tracers in both seasons was linearly correlated with aerosol acidity (pH) ( $r =$   
52  $0.421 \sim 0.752$ ), liquid water content (LWC) ( $r = 0.403 \sim 0.876$ ) and SO<sub>4</sub><sup>2-</sup> ( $r = 0.419 \sim$   
53  $0.813$ ). The results indicated that acid-catalyzed reactive uptake onto sulfate aerosol  
54 particles enhanced the formation of BSOA. In summer, the clean air mass originated  
55 from the ocean, and chlorine depletion was observed. We also found that concentrations  
56 of the total SOA tracers was correlated with HCl ( $R^2 = 0.545$ ) and chlorine ions ( $r =$   
57  $0.280 \sim 0.639$ ) in PM<sub>2.5</sub>, reflecting the contribution of Cl-initiated VOC oxidations to  
58 the formation of SOA. In winter, the northeast dominant wind direction brought  
59 continental polluted air mass to the monitoring site, affecting the transformation of  
60 BSOA tracers. This implied that anthropogenic emissions, atmospheric oxidation  
61 capacity and halogen chemistry have significant effects on the formation of BSOA in  
62 the southeast coastal area.

63 **Keywords:** SOA tracers; biogenic volatile organic compounds; anthropogenic  
64 pollutants; atmospheric oxidation capacity; coastal area  
65

## 66 **1. Introduction**

67 Secondary organic aerosol (SOA) has attracted widespread scientific research  
68 concerns, due to its potential impacts on climate change, human health and air quality  
69 (Shrivastava et al., 2017; Reid et al., 2018; Zhu et al., 2019; Wang et al., 2021b).  
70 Understanding the formation of SOA and assessing its relevance for environmental  
71 effects become an integral part of aerosol chemistry (Charan et al., 2019; Xiao et al.,  
72 2020; Palmer et al., 2022). However, due to its complex precursors and atmospheric  
73 physical or chemical processes, SOA prediction by air quality models remains highly  
74 uncertain (McFiggans et al., 2019). Therefore, it is necessary to better explore missed  
75 SOA sources and unknown SOA formation mechanisms.

76 SOA is produced by the conversion of biogenic and anthropogenic volatile organic  
77 compounds (BVOCs and AVOCs) through complex homogeneous and heterogeneous  
78 reactions (Charan et al., 2019; Xiao et al., 2020; Mahilang et al., 2021). BVOCs are the  
79 main precursors of SOA on a global scale, while AVOCs are the predominant  
80 contributor to SOA in urban areas (Hallquist et al., 2009; Wang et al., 2021a). Recently,  
81 laboratory, field and modeling studies have shown that anthropogenic emissions greatly  
82 affect the formation of BSOA (Hoyle et al., 2011; Shrivastava et al., 2019; Zhang et al.,  
83 2019b; Zhang et al., 2019c; Mahilang et al., 2021; Xu et al., 2021). Anthropogenic air  
84 pollutants, such as NO<sub>x</sub>, SO<sub>2</sub>, NH<sub>3</sub> and aerosols, could influence the conversion of  
85 BVOCs to the particulate phase and the production of nitrogen and sulfur compounds  
86 (Wang et al., 2020). NO<sub>x</sub> is one of the important drivers of SOA formation and yields  
87 during both daytime and nighttime through alternating the fate of peroxy radicals (RO<sub>2</sub>·)  
88 (Sarrafzadeh et al., 2016; Newland et al., 2021). While ·OH dominates the  
89 photochemical oxidation of BVOC during daylight hours, and NO<sub>3</sub>· becomes one of the  
90 main oxidants for biogenic SOA and organic nitrate formation at night. SO<sub>2</sub> also plays

91 an important role in changing SOA formation from BVOC photooxidation and  
92 ozonolysis through sulfuric acid formation and acid-catalyzed heterogeneous reactions  
93 (Zhao et al., 2018; Zhang et al., 2019b; Xu et al., 2021). In addition, NH<sub>3</sub> and amines  
94 can affect the SOA yields and composition through both gas-phase and heterogeneous  
95 reactions, by reacting with sulfuric or nitric acid to generate secondary inorganic  
96 aerosols (SIA) (Ma et al., 2018; Liu et al., 2021; Lv et al., 2022). However, due to  
97 complex precursors and atmospheric processes, the combined effects of anthropogenic  
98 emissions and meteorological factors on the formation of SOA are not fully understood.

99 The coastal area of southeastern China is under the East Asian monsoon control,  
100 which cause an obvious alternation of polluted and clean air masses from continental  
101 and ocean area, respectively (Wu et al., 2019; Hong et al., 2021). Also, the local  
102 geographical environment, including relatively high humidity, dense vegetation and  
103 strong atmospheric oxidation capacity, provides a good chance to study the sources and  
104 formation mechanisms of SOA. In our previous studies, ground-based observations in  
105 a mountainous forest area of this region showed that BSOA tracers were the largest  
106 contributor to SOA, and the aerosols were highly oxidized (Hong et al., 2019). However,  
107 with the development of rapid urbanization, anthropogenic emissions will be of great  
108 significance on SOA formation (Liu et al., 2020). Halogen radicals (chlorine, bromine,  
109 iodine) have an important role in tropospheric oxidants chemistry and OA formation  
110 (Wang et al., 2021c). Therefore, it is necessary to investigate the sources and formation  
111 mechanisms of SOA in coastal urban areas, and so as to provide a scientific basis for  
112 the estimation of regional SOA budgets and PM<sub>2.5</sub> pollution control.

113 In this study, a continuous PM<sub>2.5</sub> sampling campaign with a 4 h time resolution  
114 was conducted in a coastal city of southeastern China during the winter and  
115 summertime period. Seasonal, diurnal variations and SOC contributions of SOA tracers  
116 were analyzed. Atmospheric process identified by SOA tracers in different seasons  
117 were further analyzed. Finally, the combined effects of anthropogenic emissions and  
118 major environmental factors on promoting SOA formation was discussed.

## 119 **2. Materials and methods**

### 120 *2.1 Sample collection*

121 The sampling was performed at the Institute of Urban Environment, Chinese  
122 Academy of Sciences (118.06° E, 24.61° N), which is located in a suburban area of  
123 Xiamen, a coastal city of southeastern China. Detailed information of the air monitoring  
124 supersite was described in our previous study (Hong et al., 2021). Briefly, time-resolved  
125 (00:00–08:00, 08:00–12:00, 12:00–16:00, 16:00–20:00, 20:00–24:00 CST – China  
126 Standard Time) PM<sub>2.5</sub> samples were collected on the rooftop of the station (about 70m  
127 above the ground). The sampling was carried out by using a high volume (1.05 m<sup>3</sup> min<sup>-1</sup>)  
128 sampler (TH-1000C, Wuhan Tianhong, China) with a PM<sub>2.5</sub> inlet from 10 to 18 January,  
129 and from 5 to 14 July 2020. All samples were collected onto pre-baked (450 °C, 6 h)  
130 quartz fiber filters. Field blank samples were also collected. The sample filters were  
131 separately sealed in aluminum foil and stored in a freezer (–20 °C) prior to analysis.

### 132 *2.2 SOA tracers analysis by GC/MS*

133 The isoprene-derived SOA (SOA<sub>I</sub>) tracers included 2 methyltetrols (MTLs: 2-  
134 methylthreitol (MTL1) and 2-methylerythritol (MTL2)), C5-alkene triols (cis-2-  
135 methyl-1,3,4-trihydroxy-1-butene, trans-2-methyl-1,3,4-trihydroxy-1-butene, and 3-  
136 methyl-2,3,4-trihydroxy-1-butene) and 2-methylglyceric acid (MGA). The  
137 monoterpene-derived SOA (SOA<sub>M</sub>) tracers were composed of pinic acid (PA), pinonic  
138 acid (PNA), 3-hydroxyglutaric acid (HGA), 3-methyl-1,2,3-butanetricarboxylic acid  
139 (MBTCA), 3-hydro-4,4-dimethylglutaric acid (HDMGA), and 3-acetylglutaric acid  
140 (AGA). The β-caryophyllene-derived SOA (SOA<sub>C</sub>) tracer was β-caryophyllenic acid  
141 (CA), the toluene-derived SOA (SOA<sub>A</sub>) tracer was 2,3-Dihydroxy-4-oxopentanoic acid  
142 (DHOPA) and levoglucosan (LEV) as a tracer of biomass burning. Due to the lack of  
143 authentic standards, surrogate standards (including erythritol, malic acid, PA and  
144 citramalic acid) were used to compensate for unavoidable assay variance of SOA<sub>I</sub>,  
145 SOA<sub>M</sub>, SOA<sub>C</sub> and SOA<sub>A</sub> tracer in each sample during the pretreatment process,  
146 respectively (Fu et al., 2009). However, inherent low volatility of isoprene SOA tracers

147 could cause the uncertainties of using the GC/MS method, and low-volatility oligomers  
148 might break down into monomers, such as C5-alkene triols and 2-methyltetrols (Lopez-  
149 Hilfiker et al., 2016; Hu et al., 2016). Therefore, quantifying the abundance of certain  
150 SOA tracers remained a lot of uncertainties.

151 The analytical procedure of fifteen SOA tracers was published in our previous  
152 studies (Hong et al., 2019; Liu et al., 2020). Briefly, the filter samples were  
153 ultrasonically extracted with a mixture of dichloromethane and methanol (2:1, v/v) for  
154 10 min three times. The mixed extracts were filtered with a PTFE filter (0.22  $\mu\text{m}$ ), and  
155 dried with high purity  $\text{N}_2$  (99.99%), and then derivatized with 60  $\mu\text{L}$  of  
156 N,O-bis-(trimethylsilyl) trifluoroacetamide (BSTFA) with 1% trimethylsilyl chloride  
157 and 10  $\mu\text{L}$  of pyridine at 70  $^\circ\text{C}$  for 3 h. At last, 140  $\mu\text{L}$  of internal standard solution ( $^{13}$   
158 C n-alkane solution, 1.507  $\text{ng } \mu\text{L}^{-1}$ ) was added into the samples. Then, relative response  
159 factors (RRFs) of surrogate and internal standard were calculated to quantify the  
160 targeted organic tracers in each sample. Details of SOA tracer's calculated  
161 concentrations based on RRFs were presented in our previous studies (Hong et al., 2019;  
162 Liu et al., 2020).

163 Fifteen SOA tracers were determined by GC-MSD (7890A/5975C, Agilent  
164 Technologies, Inc., USA) with a DB-5 MS silica capillary column (i.d. 30 $\times$ 0.25 mm,  
165 0.25  $\mu\text{m}$  film thickness). 1  $\mu\text{L}$  sample was injected with splitless mode and high purity  
166 helium (99.999%) was used as carrier gas at a stable flow of 1.0 mL/min. The GC  
167 temperature was initiated at 100  $^\circ\text{C}$  (held for 1 min) and then to 300  $^\circ\text{C}$  at 5  $^\circ\text{C min}^{-1}$ ,  
168 and kept at 300  $^\circ\text{C}$  for 10 min. The operation mode is electron ionization (EI) mode of  
169 70 eV. The method detection limits (MDLs) for erythritol and PNA were 0.01 and 0.02  
170  $\text{ng m}^{-3}$ , respectively. The recoveries of erythritol, PNA, malic acid, PA and citramalic  
171 acid were 67 $\pm$ 2%, 73 $\pm$ 1%, 75 $\pm$ 1%, 88 $\pm$ 7% and 82 $\pm$ 8%, respectively. SOA tracers were  
172 not detected in the field blank samples.

### 173 2.3 Observations in the air monitoring supersite

174 Water-soluble inorganic ions (WSII) in  $\text{PM}_{2.5}$  ( $\text{Cl}^-$ ,  $\text{SO}_4^{2-}$ ,  $\text{NO}_3^-$ ,  $\text{Na}^+$ ,  $\text{K}^+$ ,  $\text{NH}_4^+$ ,  
175  $\text{Mg}^{2+}$ , and  $\text{Ca}^{2+}$ ) and gas pollutants ( $\text{HCl}$ ,  $\text{HONO}$ ,  $\text{HNO}_3$ ,  $\text{NH}_3$ ) were hourly measured

176 using a monitoring device for aerosols and gases in ambient Air (MARGA 2080;  
177 Metrohm Applikon B.V.; Delft, Netherlands). Internal calibration was carried out using  
178 LiBr standard solutions. The detection limit of  $\text{Cl}^-$ ,  $\text{SO}_4^{2-}$ ,  $\text{NO}_3^-$ ,  $\text{Na}^+$ ,  $\text{K}^+$ ,  $\text{NH}_4^+$ ,  $\text{Mg}^{2+}$ ,  
179 and  $\text{Ca}^{2+}$  were 0.01, 0.04, 0.05, 0.05, 0.09, 0.05, 0.06 and 0.09  $\mu\text{g m}^{-3}$ , respectively.

180 Hourly mass concentrations of  $\text{PM}_{2.5}$  and  $\text{PM}_{10}$  were measured by using a tapered  
181 element oscillating microbalance (TEOM1405, Thermo Scientific Corp., MA, USA).  
182  $\text{NO}_2$ ,  $\text{SO}_2$ , and  $\text{O}_3$  were monitored using continuous gas analyzers (TEI 42i, 43i, and  
183 49i, Thermo Scientific Corp., MA, USA). Ambient meteorological parameters  
184 including relative humidity (RH), temperature (T), wind speed (WS), and wind  
185 direction (WD) were obtained by an ultrasonic anemometer (150WX, Airmar, the  
186 USA). Photolysis frequencies were determined using a photolysis spectrometer (PFS-  
187 100, Focused Photonics Inc., Hangzhou, China), including the photolysis rate constants  
188  $J(\text{O}^1\text{D})$ ,  $J(\text{HCHO\_M})$ ,  $J(\text{HCHO\_R})$ ,  $J(\text{NO}_2)$ ,  $J(\text{H}_2\text{O}_2)$ ,  $J(\text{HONO})$ ,  $J(\text{NO}_3\_M)$  and  
189  $J(\text{NO}_3\_R)$ , and the spectral band ranged from 270 to 790 nm. Boundary layer height  
190 (BLH) based on ERA-5 reanalysis dataset was downloaded from the following link  
191 <https://www.ecmwf.int/en/forecasts/datasets/reanalysis-datasets/era5>.

#### 192 *2.4 Estimation of SOC using a tracer-based method*

193 The fraction of SOC formed by the oxidation of monoterpene, isoprene,  $\beta$ -  
194 caryophyllene and toluene was estimated using a tracer-based method (Kleindienst et  
195 al., 2007; Hong et al., 2019). It is defined as  $[\text{SOC}] = \sum i[\text{tri}]/f_{\text{SOC}}$ , where [SOC]  
196 represents the mass concentration of SOC ( $\mu\text{gC m}^{-3}$ ) and  $\sum i[\text{tri}]$  means the sum of the  
197 concentration of individual SOA tracer ( $\mu\text{g m}^{-3}$ ). The carbon mass fractions ( $f_{\text{SOC}}$ ) of  
198 monoterpene, isoprene,  $\beta$ -caryophyllene and toluene were  $0.231 \pm 0.111$ ,  $0.155 \pm 0.039$ ,  
199  $0.023 \pm 0.005$  and  $0.008 \pm 0.003$ , respectively, based on smog-chamber experimental  
200 data (Kleindienst et al., 2007).

#### 201 *2.5 Aerosol acidity and OH calculation*

202 The forward mode of ISORROPIA II thermodynamic model was used to calculate  
203 the aerosol acidity (pH) (Fountoukis and Nenes, 2007). ISORROPIA II can calculate

204 liquid water content (LWC), based on total  $\text{SO}_4^{2-}$ ,  $\text{NO}_3^-$  (gas  $\text{HNO}_3$  plus particle  $\text{NO}_3^-$ ),  
 205  $\text{Cl}^-$ , ammonia (gas  $\text{NH}_3$  plus particle  $\text{NH}_4^+$ ), non-volatile cations ( $\text{Na}^+$ ,  $\text{K}^+$ ,  $\text{Ca}^{2+}$ ,  $\text{Mg}^{2+}$ ),  
 206 and meteorological factors (RH and T) (Rumsey et al., 2014; Guo et al., 2016). The pH  
 207 value from ISORROPIA II was calculated using the following equation:

$$208 \quad \text{pH} = -\lg\left(\frac{1000 \times \text{H}^+}{\text{LWC}}\right)$$

209 where  $\text{H}^+$  is the hydronium ion concentration loading for an air sample ( $\mu\text{g}/\text{m}^3$ ).

210 The OH concentration ( $[\text{OH}]$ ) was estimated using the  $\text{NO}_2$  and HONO  
 211 concentrations and the photolysis rate constants (J) of  $\text{NO}_2$ ,  $\text{O}_3$ , and HONO, according  
 212 to the following improved empirical formula (Wen et al., 2019).

$$213 \quad [\text{OH}] = 4.1 \times 10^9 \times \frac{J(\text{O}^1\text{D})^{0.83} \times J(\text{NO}_2)^{0.19} \times (140 \times \text{NO}_2 + 1) + \text{HONO} \times J(\text{HONO})}{0.41 \times \text{NO}_2^2 + 1.7 \times \text{NO}_2 + 1 + \text{NO} \times k_{\text{NO}+\text{OH}} + \text{HONO} \times k_{\text{HONO}+\text{OH}}}$$

## 214 2.6 Statistical analysis

215 Correlation analysis by SPSS 22.0 software (IBM, Armonk, NY, USA) was used  
 216 to study the relationship among SOA tracers, meteorological parameters and criteria air  
 217 pollutants. One-way analysis of variance (ANOVA) was adopted to examine the  
 218 variations of different factors.

## 219 2.7. Backward trajectory analysis

220 Hybrid Single-Particle Lagrangian Integrated Trajectory (HYSPLIT) was used to  
 221 analyze the impacts of air masses on Xiamen during different seasons. 72 h backward  
 222 trajectories were calculated every hour at a height of 500 m. The meteorological data  
 223 with a resolution of  $1^\circ$  longitude  $\times$   $1^\circ$  latitude was obtained from the NCEP/GDAS.  
 224 Cluster analysis was adopted using the total spatial variance (TSV).

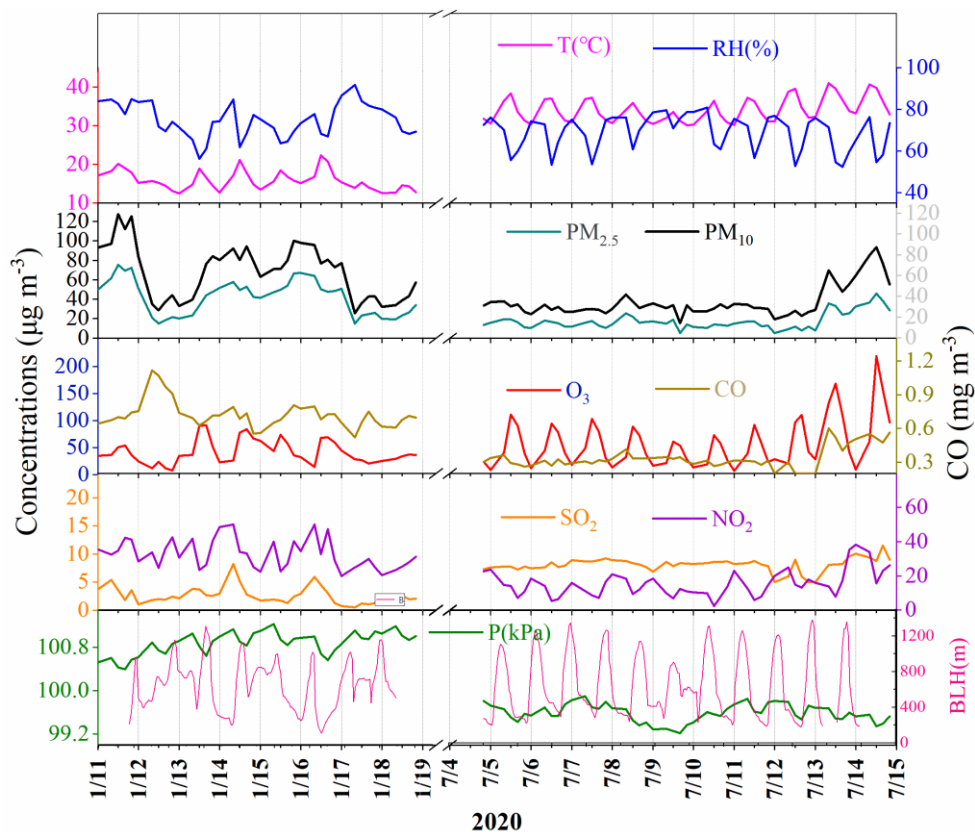
# 225 3 Results and discussion

## 226 3.1. Overview of air pollutants

227 The concentrations of criteria air pollutants, including  $\text{SO}_2$ , CO,  $\text{NO}_2$ ,  $\text{O}_3$ ,  $\text{PM}_{2.5}$   
 228 and  $\text{PM}_{10}$ , and meteorological parameters during wintertime and summertime were  
 229 shown in Fig.1. The concentrations of  $\text{PM}_{2.5}$  in winter ranged from 14.9 to  $75.3 \mu\text{g m}^{-3}$   
 230 with an average of  $42.1 \mu\text{g m}^{-3}$ , which was much higher than that (the average of 18.4



231  $\mu\text{g m}^{-3}$ ) in summer, ranging from 12.8 to 46.4  $\mu\text{g m}^{-3}$ . The concentrations of CO, NO<sub>2</sub>  
 232 and PM<sub>10</sub> showed similar seasonal trends to the pattern of PM<sub>2.5</sub>. In contrast, O<sub>3</sub> had the  
 233 highest concentration in summer, which was attributed to the formation of  
 234 photochemical reaction under strong UV radiation and the weak titration of nitrogen  
 235 oxides. Meanwhile, the concentrations of SO<sub>2</sub> ( $8.37\pm 0.79 \mu\text{g m}^{-3}$ ) in summer was also  
 236 higher than that ( $2.63\pm 1.95 \mu\text{g m}^{-3}$ ) in winter, mainly attributed to the influence of coal  
 237 combustion and ship emissions. The monitoring site was located approximately 15 km  
 238 away from Xiamen port area and a coal-fired power plant ( $4 \times 300 \text{ kW}$ ) in the south.  
 239 Southerly winds were prevailed in summer, which might cause the relative high  
 240 concentration of SO<sub>2</sub> in the monitoring site.



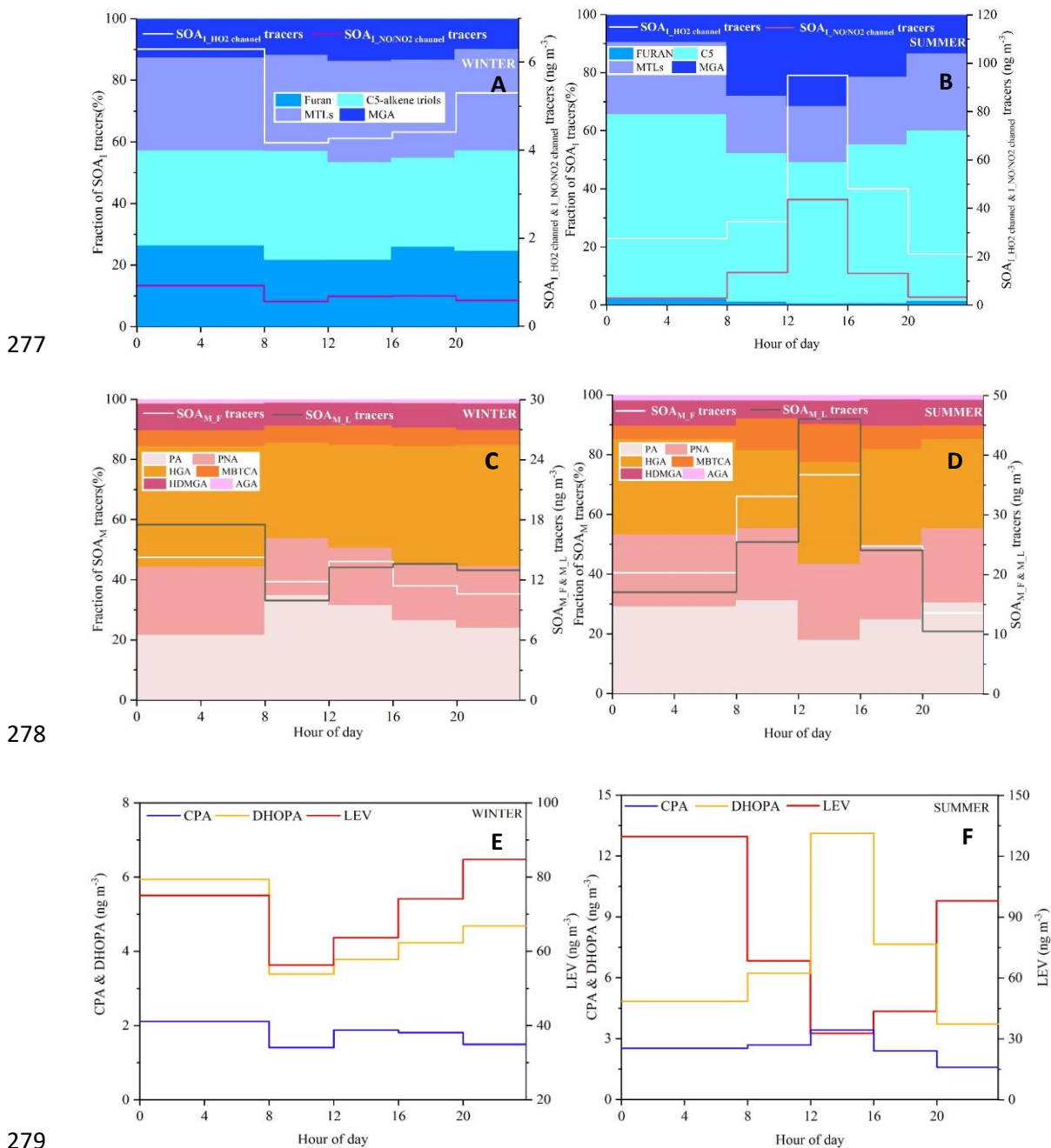
241  
 242 **Figure 1. Time series of criteria air pollutants and meteorological parameters**  
 243 **during the sampling period**

244 *3.2 Temporal variations of SOA tracers and estimated SOC*

245 Temporal variations of individual SOA tracer are shown in Fig.S1. The average  
 246 concentrations of total SOA tracers in winter and summer were 37.3 and 111.3  $\text{ng m}^{-3}$ ,

247 respectively. The predominance of SOA<sub>M</sub> (26.6 ng m<sup>-3</sup>), followed by ASOA (4.60 ng  
248 m<sup>-3</sup>), SOA<sub>I</sub> (4.35 ng m<sup>-3</sup>) and SOA<sub>C</sub> (1.76 ng m<sup>-3</sup>) was observed in winter while SOA<sub>I</sub>  
249 (54.4 ng m<sup>-3</sup>) and SOA<sub>M</sub> (47.8 ng m<sup>-3</sup>) in summer were the main contributors to total  
250 SOA tracers, followed by ASOA (6.64 ng m<sup>-3</sup>) and SOA<sub>C</sub> (2.45 ng m<sup>-3</sup>). In summer,  
251 BSOA tracers showed much higher concentrations in the daytime (149.3 ng m<sup>-3</sup>) than  
252 in the nighttime (60.1 ng m<sup>-3</sup>), while inverse results were observed in winter (30.4 ng  
253 m<sup>-3</sup> and 35.0 ng m<sup>-3</sup> in the daytime and nighttime, respectively). As shown in Table S2,  
254 in summer, SOA<sub>I</sub> in the daytime ranged from 21.3 to 293.2 ng m<sup>-3</sup> (average of  
255 82.0±66.2 ng m<sup>-3</sup>) and the concentrations of SOA<sub>I</sub> ranging from 6.81 to 110.1 ng m<sup>-3</sup>  
256 (average of 26.8±24.6 ng m<sup>-3</sup>) were observed in the nighttime. However, in winter, the  
257 concentrations of isoprene SOA tracers in the daytime ranging from 1.36 to 11.1 ng m<sup>-3</sup>  
258 (average of 3.79±2.37ng m<sup>-3</sup>) were lower than those (average of 4.91±3.75 ng m<sup>-3</sup>) in  
259 the nighttime. As shown in Fig. 2, diurnal variations of SOA<sub>M</sub>, SOA<sub>I</sub>, CPA and DHOPA  
260 tracers in summer showed high levels in the afternoon (12:00–16:00 CST), due to the  
261 impacts of beneficial photochemical oxidation conditions caused by high temperature  
262 and strong UV radiation. The related SOA tracers were consisted with the emissions of  
263 their precursors including biogenic and anthropogenic VOCs, similar to our previous  
264 studies (Hong et al., 2019; Liu et al., 2020). However, the SOA tracers in winter showed  
265 the lowest concentrations in the morning (8:00–12:00 CST), related with the favorable  
266 dispersion conditions caused by the increasing planetary boundary layer height (BLH)  
267 (Fig.1). Levoglucosan (LEV), a typical tracer of biomass burning, similar seasonal and  
268 diurnal trend to other tracers was observed. However, LEV may not be as stable in the  
269 atmosphere, especially under high relative humidity conditions (Hoffmann et al., 2010).  
270 In this study, maybe, it's hard to reflect the real concentration of LEV. A correlation of  
271 CPA with LEV was carried out (Fig.S2), just to discuss the impacts of biomass burning  
272 on the distribution of CPA tracers through local or long-range transport. Totally, high  
273 concentrations of BSOA tracers was found in the daytime and in summer, indicating  
274 the effects of temperature on biogenic VOCs emissions and their photochemical  
275 oxidations. And the concentrations of BSOA tracers in winter increased in the nighttime,

276 due to the changing of nocturnal boundary layer.



277  
278  
280 **Figure 2. Diurnal variation of individual SOA tracer during the wintertime (A,**  
281 **C, and E) and summertime (B, D, and F)**

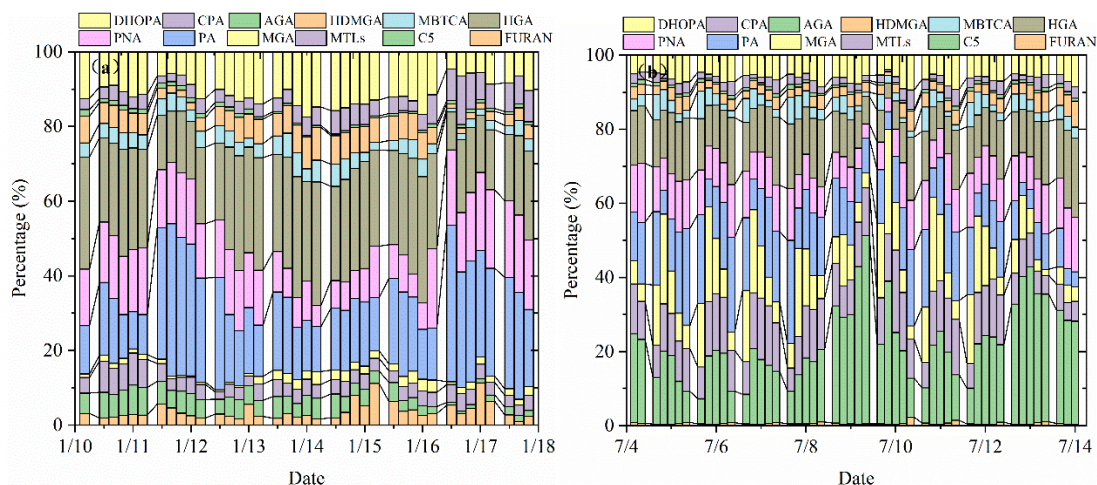
282 As shown in Fig.S2a, b, SOA tracers-based SOC in winter and summer was  
283 estimated. The concentrations of SOC in summer was higher than that in winter,  
284 attributed to the increase of flourishing vegetation emissions and photochemical reactions  
285 under high temperature and strong solar radiation conditions. For individual SOA tracer, the

286 concentrations of monoterpene-derived SOC was comparable to the toluene-derived  
287 SOC, which were higher than isoprene-derived SOC and  $\beta$ -caryophyllene-derived SOC.  
288 An obvious trend of diurnal variations of isoprene-derived SOC in summer was  
289 observed, which was consistent with the diurnal pattern of isoprene concentration  
290 (Fig.S3). However, no similar trend was found in winter, attributed to the influence of  
291 low temperature on inhibiting the emissions of isoprene from various kinds of plants.  
292 In addition, the toluene, monoterpene, isoprene and  $\beta$ -caryophyllene-derived SOC in  
293 summer accounted for 40.0%, 39.2%, 15.7% and 5.1% of the total SOC, respectively  
294 (Fig.S2c, d). However, in winter, the percentages of toluene, monoterpene, isoprene  
295 and  $\beta$ -caryophyllene-derived SOC were 47.2%, 42.1%, 3.2% and 7.6%, respectively.  
296 The percentages of isoprene-derived SOC estimated from different precursors varied  
297 significantly among the seasons. High temperature enhanced the emissions of isoprene,  
298 and strong solar radiation favored the formation of isoprene SOA tracers, contributing  
299 to the highest isoprene-derived SOC percentage in summer (Ding et al., 2014). And the  
300 highest percentages of toluene-derived SOC (47.2%) in winter were related with  
301 anthropogenic emissions and adverse diffusion conditions.

### 302 *3.3 Atmospheric process indication of BSOA tracers*

303 As shown in Fig.3, percentages of different types of SOA tracers in winter and  
304 summer were calculated. In summer, the monoterpene, isoprene, toluene and  $\beta$ -  
305 caryophyllene SOA tracers accounted for 45.8%, 45.6%, 6.2% and 2.3% of the total  
306 SOA tracers, respectively. However, in winter, the percentages of monoterpene,  
307 isoprene, toluene and  $\beta$ -caryophyllene SOA tracers were 70.1%, 14.0%, 11.0% and  
308 4.9%, respectively. The percentage of SOA<sub>I</sub> tracers decreased sharply, due to the  
309 impacts of temperature on isoprene emissions, which was consisted with our previous  
310 findings (Hong et al., 2019). Meanwhile, the concentrations of SOA<sub>M</sub> tracers were the  
311 largest in both seasons, due to a large amount of monoterpene emissions from the  
312 related plant species. Xiamen, an international garden city, located in coastal area of  
313 southeastern China. Monoterpene, such as  $\alpha/\beta$ -pinene, is mostly emitted by coniferous  
314 plant and most flowers and fruits, while isoprene originates from broad-leaved trees

315 and deciduous plants (Ding et al., 2014; Shrivastava et al., 2017; Yang et al., 2021).



316

317 **Figure 3. Percentages of isoprene, monoterpene,  $\beta$ -caryophyllene and toluene**  
318 **SOA tracers in winter (a) and summer (b)**

319 The first (PA and PNA) and later generation (HGA, AGA, HDMGA and MBTCA)  
320 products were used to evaluate the aging degree of SOA<sub>M</sub> (Ding et al., 2014; Hong et  
321 al., 2019). In this study, HGA (32.2%) was the major component of  $\alpha/\beta$ -pinene tracers,  
322 followed by PA (30.5%), PNA (21.8%), HDMGA (7.3%), MBTCA (6.8%), and AGA  
323 (1.5%). The percentage of PA and PNA were much higher than those in mountainous  
324 background areas (PA: 9% and PNA: 3%)(Hong et al., 2019), suggesting the  
325 contribution of preliminary products to SOA in urban areas. As shown in Fig.3, the  
326 percentages of PA and PNA in winter (21.8% and 14.2%) were higher than those in  
327 summer (14.2% and 10.7%). Reacted with atmospheric oxidants including O<sub>3</sub> and OH,  
328 PA and PNA were transformed into MBTCA (Offenberg et al., 2007). This is the reason  
329 why the proportions of PA and PNA had a significant decreasing trend from winter to  
330 summer. The ratio of MBTCA/(PA+PNA) in summer and winter were 0.16±0.09 and  
331 0.12±0.07, respectively, which also proved the impacts of atmospheric oxidation  
332 capacity on the aging degree of SOA<sub>M</sub>. In addition, the ratio of HGA/MBTCA could  
333 be used to distinguish the contribution of  $\alpha$ -pinene or  $\beta$ -pinene to the SOA<sub>M</sub> formation  
334 (Jaoui et al., 2005; Ding et al., 2014). Low ratio of HGA/MBTCA (~1.0) showed that  
335  $\alpha$ -pinene was the major precursor for SOA<sub>M</sub> (Lewandowski et al., 2013). The ratio of

336 HGA/MBTCA with an average of 5.78 in Xiamen was high, suggesting the contribution  
337 of  $\beta$ -pinene to SOA<sub>M</sub>.

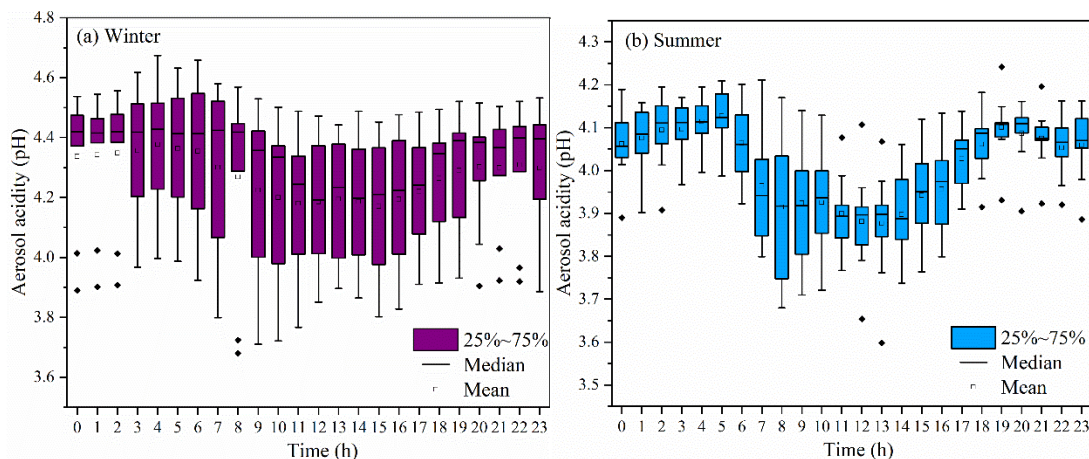
338 As shown in Fig.3, MTLs and C5 alkene triols were the main components of the  
339 total SOA<sub>I</sub>, with an average percentage of  $68.0\pm 14.9\%$ , indicating a low-NO<sub>x</sub>  
340 environment (Ding et al., 2014; Liu et al., 2020). In summer, the percentages of MTLs  
341 and C5 alkene triols to the total SOA tracers in summer (21.8% and 14.2%) were  
342 obviously higher than those in winter (4.2% and 4.3%). This was consisted with the  
343 fact that the concentrations of NO<sub>2</sub> ( $14.8\pm 7.46 \mu\text{g m}^{-3}$ ) in summer was significantly  
344 lower than that ( $32.7\pm 32.6 \mu\text{g m}^{-3}$ ) in winter. Previous studies found that MTLs and C5  
345 alkene triols were formed by the OH and HO<sub>2</sub> radicals via the HO<sub>2</sub> channel under low-  
346 NO<sub>x</sub> conditions (Surratt et al., 2010). C5 alkene triols are mainly produced by acid  
347 catalyzed reaction of Isoprene Epoxydiols (IEPOX) in the gas phase, while MTLs are  
348 formed by ring opening products of IEPOX (Surratt et al., 2007; Surratt et al., 2010).  
349 And the ozonolysis of isoprene was also an important pathway for MTLs in the  
350 presence of acid sulfate aerosols (Riva et al., 2016).

351 CPA, the typical tracer of sesquiterpenes, is formed by the photooxidation of  $\beta$ -  
352 caryophyllene (Jaoui et al., 2007). As shown in Fig.3, CPA in winter and summer  
353 accounted for 5.0% and 2.3% of the total SOA tracers, respectively. This is because  
354 that the percentage of SOA<sub>I</sub> has significant increase in summer. And the concentrations  
355 of CPA ( $2.5\pm 2.0 \text{ ng m}^{-3}$ ) in summer were higher than that ( $1.7\pm 0.8 \text{ ng m}^{-3}$ ) in winter,  
356 probably attributed to the emissions of  $\beta$ -caryophyllene driven by temperature and solar  
357 radiation. The CPA has a good correlation with DHOPA in summer (Fig.S4),  
358 suggesting the influence of photochemical oxidation (Liu et al., 2020). However, the  
359 CPA were not correlated with LEV in both seasons, reflecting the limited contribution  
360 of biomass burning (Zhang et al., 2019c).

#### 361 *3.4 Impacts of aerosol acidity on BSOA formation*

362 Aerosol acidity (pH) was an important factor on SOA formation (Surratt et al.,  
363 2007; Offenberg et al., 2009; Zhang et al., 2019b; Zhang et al., 2019d). Time series of  
364 aerosol pH calculated by ISORROPIA II is shown in Fig.4. The PM<sub>2.5</sub> in Xiamen was

365 moderately acidic with daily pH range from 3.68 to 4.67. The highest aerosol pH was  
 366 observed in winter, and the lowest pH in summer. This is with similar seasonal trend,  
 367 closing to the Yangtze River Delta (YRD) region, but obviously lower levels than those  
 368 in NCP cities of China (Zhou et al., 2021). In general, the aerosol pH in Chinese cities  
 369 were higher than those in US and European.



370

371 **Figure 4. Diurnal variations of aerosol acidity (pH) during the wintertime (a)**  
 372 **and summertime (b) period (The boxes with error bars represent the 10th, 25th,**  
 373 **75th, and 90th percentiles)**

374 A declining trend pH during the daytime was observed (Fig. 4), which was related  
 375 to the changes of chemical compositions and environmental conditions. The aerosol pH  
 376 levels (~3 to 6) was related with a shift from sulfate- to nitrate-dominated aerosols (Guo  
 377 et al., 2017). According to the multiphase buffer theory, the peak buffer pH ( $pK_a^*$ )  
 378 regulated the aerosol pH, and temperature could obviously cause the variation of  
 379 aerosol pH (Zheng et al., 2020). To further discuss the impacts of aerosol acidity on  
 380 BSOA formation in coastal city, we analyzed the relationship between BSOA tracers  
 381 and seed particles with different pH and liquid water content (LWC) (Fig. S5 and Table  
 382 1).

**Table 1 Correlations between individual BSOA tracer and environmental factors in winter and summer**

Season	SOA tracer	pH	LWC	HONO	PM <sub>2.5</sub>	Cl <sup>-</sup>	NO <sub>3</sub> <sup>-</sup>	SO <sub>4</sub> <sup>2-</sup>	NH <sub>3</sub>	SO <sub>2</sub>	NO <sub>2</sub>	Ox	T	RH	UV
WINTER (n=39)	C5	.584**	.701**	.534**	.690**	.569**	.710**	.663**	.705**	0.308	.353*	0.203	.361*	0.140	0.200
	MTLS	.590**	.705**	.431*	.665**	.639**	.707**	.651**	.757**	0.185	0.229	0.098	.353*	0.295	-0.068
	MGA	.390*	.707**	0.261	.668**	0.081	.758**	.572**	0.284	0.172	0.123	.374*	.377*	-0.019	0.238
	PA	.432*	.403**	.463**	.407**	.481*	.416*	.488*	.440*	.446*	0.241	-0.193	.319*	-0.205	0.145
	PNA	.489**	.579**	0.311	.459**	.516**	.573**	.533**	.543**	0.08	0.071	-0.101	0.121	.337*	-0.122
	HGA	.443*	.829**	.352*	.834**	.600**	.847**	.754**	.641**	0.275	0.299	.451**	.451**	0.043	0.210
	MBTCA	.433*	.678**	.447**	.670**	.435*	.733**	.589**	.710**	.327*	0.253	.492**	.552**	-0.158	0.317
	HDMGA	.421*	.876**	.401*	.867**	.631**	.884**	.813**	.643**	.335*	.321*	.526**	.485**	-0.049	0.327
	AGA	.570**	.575**	.370*	.488**	.577**	.566**	.544**	.731**	0.126	0.181	0.019	0.279	0.298	-0.122
	CPA	0.212	.462**	-0.068	.452**	.483**	.437*	.419*	.255	-0.15	-0.170	0.016	0.079	0.200	-0.144
SUMMER (n=50)	C5	-.495**	.425**	0.160	.622**	-.340*	0.268	.625**	.436**	0.254	0.025	.649**	.573**	-.529**	0.247
	MTLS	-.551**	0.131	0.055	0.272	-.439**	0.131	.428**	.304*	0.089	-0.278	.550**	.610**	-.594**	0.263
	MGA	-.540**	0.029	0.116	0.132	-.403**	0.066	.472**	0.270	0.096	-0.410**	.443**	.633**	-.668**	.382*
	PA	-.633**	.483**	.601**	.461**	-0.135	.541**	.502**	.405*	0.037	0.238	.456**	.626**	-.558**	.400*
	PNA	-.664**	.616**	.387**	.812**	-.389**	.450**	.784**	.503**	0.269	.294*	.769**	.718**	-.631**	.404*
	HGA	-.607**	.612**	.299*	.836**	-.384**	.447**	.770**	.539**	.316*	0.272	.808**	.670**	-.599**	0.322
	MBTCA	-.752**	.415**	0.237	.577**	-.382**	.359*	.636**	.501**	0.201	-0.052	.712**	.852**	-.816**	.588**
	HDMGA	-.525**	.618**	.299*	.833**	-.342*	.408**	.768**	.488**	.358*	.365**	.746**	.574**	-.500**	0.240
	AGA	-.684**	.592**	.447**	.766**	-.334*	.479**	.735**	.435**	0.244	0.271	.694**	.720**	-.634**	.477**
	CPA	-.552**	.625**	.441**	.780**	-.280*	.453**	.763**	.307*	.299*	.503**	.611**	.529**	-.458**	0.305

\*/\*\*Correlation coefficients with an asterisk indicate statistically significant relationships at  $\alpha = 0.05$ , and two asterisks mean significant at  $\alpha = 0.01$ .



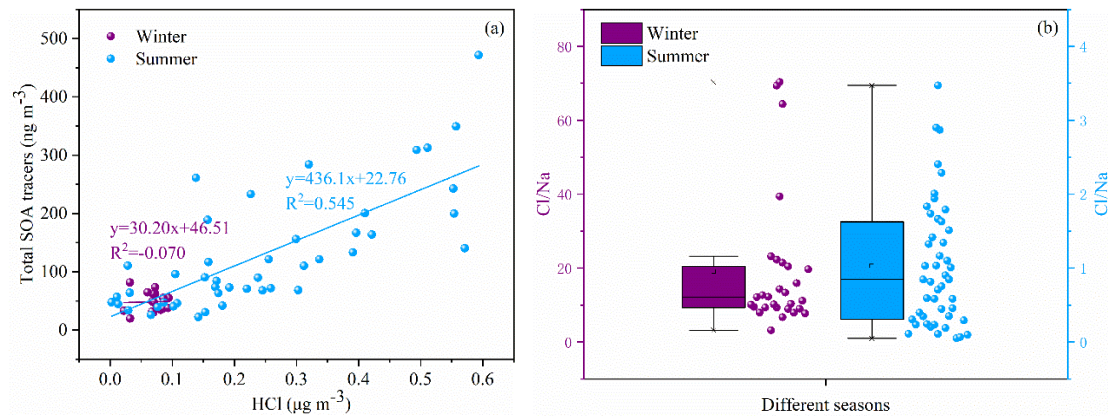
387 In Table 1, the BSOA tracers was linearly correlated with aerosol acidity (pH) and  
388  $\text{SO}_4^{2-}$ . In summer, BSOA tracers in the particle phase were found to increase with  
389 increasing acidity, which was attributed to the presence of acid catalyzed aerosols. For  
390 example, isoprene SOA tracers is mainly formed through acid-catalyzed reactive uptake  
391 of isoprene-derived epoxydiols (IEPOX) onto sulfate aerosol particles. In our previous  
392 studies, we have reported that high concentration of MTLs was related with sulfate,  
393 which could significantly promote the formation of isoprene-SOA tracers (Liu et al.,  
394 2020). Other studies also found that sulfate could increase the BSOA production by  
395 promoting acid-catalyzed ring-opening reactions (Xu et al., 2015). In contrast, positive  
396 correlations between BSOA tracers and aerosol pH in winter were observed, indicating  
397 that the formation of BSOA was predominantly enhanced by other factors, except for  
398 the aerosol acidity. The aerosol pH in winter was higher than those in summer, probably  
399 due to the influence of nitrate-dominated aerosols. Also, the aged aerosols through long-  
400 range transport might result in the increase of BSOA tracers and aerosol pH.

401 In addition, positive correlation between BSOA tracers and LWC was observed  
402 (Table 1), probably attributed to the effects of the LWC on determining the peak buffer  
403 pH ( $\text{pK}_a^*$ ). Zheng et al. (2020) reported that the buffering effect of ammonia suppresses  
404 the contribution of different chemical compositions in aerosol particles, making LWC  
405 the primary determinant of aerosol pH. Other studies have demonstrated that the uptake  
406 coefficient of first-generation oxidation products, especially for carbonyl compounds,  
407 might depend on RH (Luo et al., 2019). Meanwhile, high LWC could reduce the aerosol  
408 particle viscosity, which was benefit to the generation of the reactive intermediate such  
409 as IEPOX, or other oxidation products of VOC into aqueous-phase of aerosol particles,  
410 thereby promoting the formation of BSOA (Zhang et al., 2019b; Zhang et al., 2019d).

### 411 *3.5 Impacts of chlorine on BSOA formation*

412 Halogen radicals (Cl, Br and I) originated from sea salt aerosol (SSA) have an  
413 important role in tropospheric oxidants chemistry (Wang et al., 2021c). In this study,  
414 chlorine depletion was frequently observed in summer (Fig.5b), indicating that HCl can  
415 be formed through acid displacement of sea salt aerosol  $\text{Cl}^-$  by  $\text{H}_2\text{SO}_4$  and  $\text{HNO}_3$   
416 produced from anthropogenic emissions of  $\text{SO}_2$  and  $\text{NO}_x$ . Moreover, concentrations of  
417 the total SOA tracers were positively correlated with HCl (Fig.5a), suggesting the  
418 enhancement of SOA precursors transformation. Previous studies have found that Cl-  
419 initiated VOC oxidations could contribute to the formation of SOA (Wang and Ruiz,

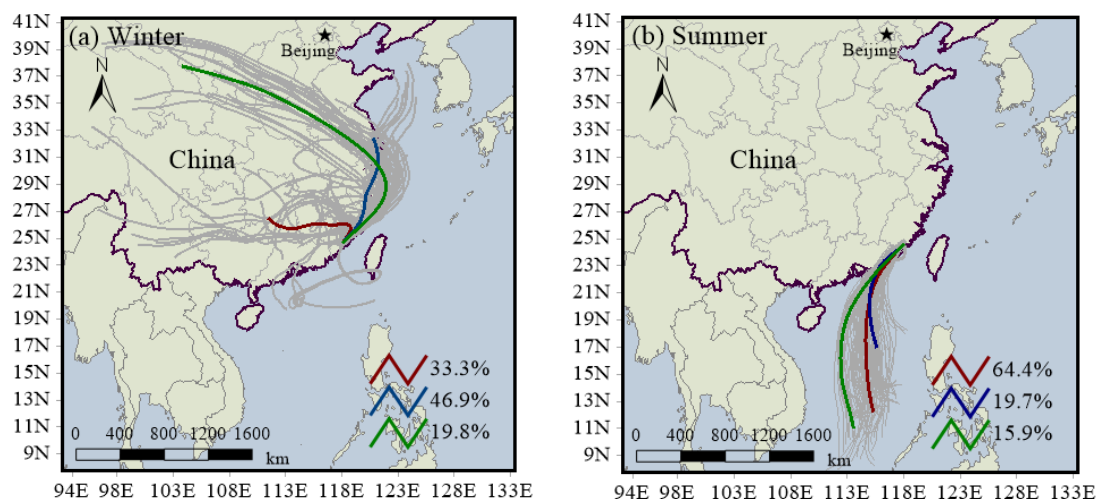
420 2017; Dhulipala et al., 2019).



421

422 **Figure 5. Correlations of total SOA tracers and HCl (a) and chlorine depletion**  
423 **(b) in different seasons**

424 Under ammonia-rich conditions, HCl partitioned into the aqueous particulate  
425 phase mostly took place, and chlorine ions could affect aqueous oxidation of secondary  
426 organic compounds (Xu et al., 2021). As shown in Table 1, most of SOA tracers in  
427 winter were correlated with the concentrations of chlorine ions in PM<sub>2.5</sub>, while inverse  
428 results were observed in summer. In winter, the dominant wind direction is northeast  
429 (Fig.6), and chlorine mainly come from continental polluted air mass, such as industrial  
430 and combustion emissions. So, anthropogenic pollutants through long-range transport  
431 might cause the enhancement of SOA tracer concentrations at the monitoring site.  
432 However, in summer, negative correlations of BSOA tracers and chlorine ions in PM<sub>2.5</sub>  
433 was found, probably due to the influence of chlorine depletion. As shown in Fig. 6, the  
434 dominant wind direction is southerly, and chlorine mainly originated from the spray of  
435 sea salt.



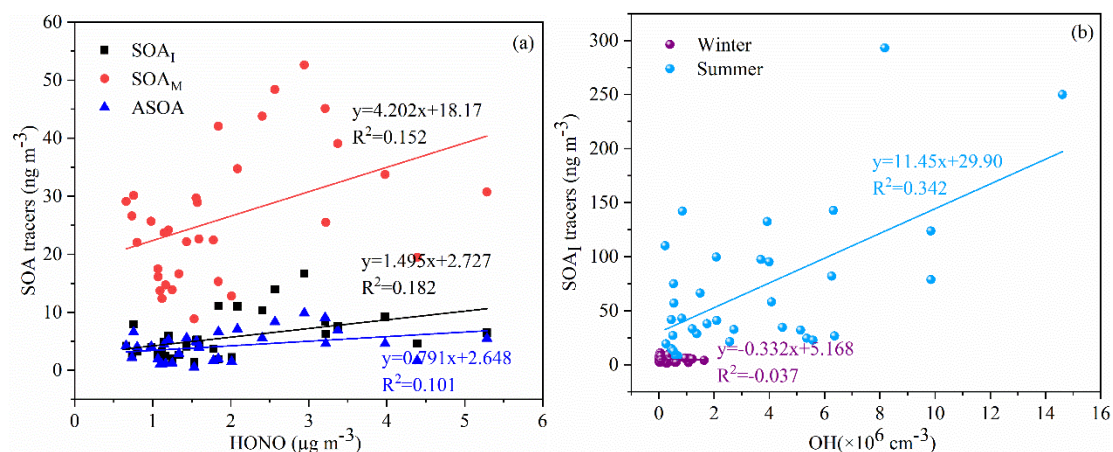
436

437 **Figure 6. Backward trajectories analyses during the winter (a) and summertime**  
 438 **(b)**

439 *3.6. Enhanced formation of BSOA by anthropogenic emissions*

440 Recent studies had indicated that anthropogenic emissions might affect SOA  
 441 formation through multiple chemical processes, based on laboratory studies and field  
 442 observations (Kari et al., 2019; Shrivastava et al., 2019; Zhang et al., 2019c; Cheng et  
 443 al., 2021; Xu et al., 2021). In this study, we conducted the correlation analysis of  
 444 individual SOA tracers and Ox (=O<sub>3</sub>+NO<sub>2</sub>), HONO, OH, SO<sub>2</sub>, NH<sub>3</sub>, PM<sub>2.5</sub>, sulfate,  
 445 nitrate, as well as meteorological parameters (including T, RH and UV) (Table 1).

446 Most of SOA tracers have a significant positive correlation with NH<sub>3</sub>, suggesting  
 447 an enhancement effect on the formation of SOA (Table 1). NH<sub>3</sub> could affect the SOA  
 448 yields through both gas-phase and heterogeneous reactions (Na et al., 2007; Ma et al.,  
 449 2018; Hao et al., 2020). Gas-phase reaction between NH<sub>3</sub> and organic acids (such as  
 450 PA and PNA) produced ammonium salts in the particle phase, which contributed to the  
 451 increased SOA formation. However, not all gas-phase organic acids (e.g., MGA and  
 452 pyruvic acid) could demonstrate gas-to-particle conversion (Na et al., 2007). When  
 453 SOA formation had ceased, the addition of excessive NH<sub>3</sub> would result in the rapid  
 454 decomposition of the main SOA species, due to the nucleophilic attack of NH<sub>3</sub> (Ma et  
 455 al., 2018).



456

457 **Figure 7. Relationships of SOA tracers and HONO (a) and its estimated OH (b)**

458 As an indicator of atmospheric oxidation capacity, the tropospheric odd oxygen  
 459 O<sub>x</sub> (O<sub>3</sub>+NO<sub>2</sub>) was calculated. As shown in Table 1, the majority of SOA tracers in  
 460 summer showed significant positive correlations with O<sub>x</sub> (R>0.5, P<0.001). However,  
 461 in winter, a part of SOA<sub>M</sub> tracers (e.g. HGA, MBTCA and HDMGA) were found to be  
 462 significantly correlated with O<sub>x</sub>. In addition, HONO and OH radicals, another critical  
 463 indicator of atmospheric oxidation capacity, was also discussed. In this study, the  
 464 concentration of OH radicals calculated from HONO in summer was higher than those  
 465 in winter. In summer, the SOA<sub>I</sub> tracers was correlated with OH radicals (Fig.7b),  
 466 consisted with previous findings that OH radicals could promote the formation of SOA  
 467 (Sarrafzadeh et al., 2016; Liu et al., 2019; Song et al., 2019; Zhang et al., 2019a). Due  
 468 to its photolysis to produce OH radicals during the daytime, HONO could facilitate  
 469 SOA formation. In winter, the concentrations of SOA<sub>I</sub>, SOA<sub>M</sub> and ASOA tracers were  
 470 correlated with HONO (Fig.7a). These results indicated high concentrations of HONO  
 471 and sufficient ultraviolet radiation could enhance the photochemical reactions of VOCs.  
 472 Which was consisted with our previous results on the formation of peroxyacetyl nitrate  
 473 (PAN) (Hu et al., 2020). As for T and UV, it exhibited significantly positive correlations  
 474 with the related SOA tracers, especially in summer. These results suggested that SOA  
 475 tracers were produced from the photo-oxidation of VOC precursors (Cheng et al., 2021).

476 In addition, the SOA tracers were significantly positive correlated with PM<sub>2.5</sub> and  
 477 its components including NO<sub>3</sub><sup>-</sup> and SO<sub>4</sub><sup>2-</sup>. In coastal cities of southeastern China, with  
 478 the development of rapid urbanization, air pollution caused by motor vehicles and  
 479 industrial emissions is becoming more frequent in winter (Wu et al., 2020). The Xiamen  
 480 port is one of the top 10 ports in China, resulting the impacts of ship emissions and port

481 activities on ambient air quality (Xu et al., 2018), and the numbers of motor vehicles  
482 increased sharply in recent years. We also found that the 90th percentile of maximum  
483 daily average 8h (MDA8) O<sub>3</sub> concentrations in Xiamen was significantly increased  
484 from 2015 to 2020 (Fig. S6). During the past several years, the elevated secondary  
485 inorganic components, including NO<sub>3</sub><sup>-</sup>, SO<sub>4</sub><sup>2-</sup> and NH<sub>4</sub><sup>+</sup>, accounted for 40-50% of the  
486 total PM<sub>2.5</sub>, and OM ranged from 30% to 40% (Wu et al., 2019; Hong et al., 2021).  
487 These results also implied the effects of anthropogenic emissions and enhanced  
488 atmospheric oxidation capacity on secondary formation of aerosol particles under  
489 atmospheric stagnant conditions.

## 490 **Conclusions**

491 Pollution characteristics and source identification of BSOA tracers during the  
492 summer and winter in coastal areas of southeastern China were investigated. The  
493 average concentration of total BSOA tracers in summer was higher than that in winter,  
494 with the predominance of SOA<sub>M</sub>, followed by SOA<sub>I</sub> and SOA<sub>C</sub>. The BSOA tracers in  
495 summer were predominantly produced by the influence of photochemical oxidation  
496 under relatively clean conditions. However, in winter, the formation of BSOA tracers  
497 were attributed to the impacts of anthropogenic emissions and atmospheric stagnant  
498 conditions. In addition, the results also indicated that acid-catalyzed reactive uptake  
499 onto sulfate aerosol particles enhanced the formation of BSOA in both seasons. We  
500 further found that Cl-initiated VOC oxidations has potentially accelerated the  
501 transformation of BSOA precursors through sea salt aerosol originated from the ocean  
502 in summer and anthropogenic emissions in winter. This study demonstrated that the  
503 combined effects of anthropogenic pollutants and atmospheric oxidation capacity on  
504 the formation of BSOA in coastal area.

505

506 **Data Availability.** The data set related to this work can be accessed via  
507 <https://doi.org/10.5281/zenodo.6376025> (Hong, 2022). The details are also available  
508 upon request from the corresponding author (ywhong@iue.ac.cn).

509

510 **Authorship Contribution Statement.** Youwei Hong and Xinbei Xu contributed equally  
511 to this work. Youwei Hong designed and wrote the manuscript. Xinbei Xu collected the  
512 data, contributed to the data analysis. Dan Liao, Taotao Liu, Xiaoting Ji and Ke Xu  
513 performed modeling analyses and data analysis. Jinsheng Chen supported funding of

514 observation and research. Chunyang Liao, Ting Wang and Chunshui Lin contributed to  
515 revise the manuscript.

516

517 **Competing interests.** The authors declare that they have no conflict of interest.

518

519 **Acknowledgement.** The authors gratefully acknowledge Yanting Chen, Han Zhang and  
520 Xu Liao (Institute of Urban Environment, Chinese Academy of Sciences) for the  
521 guidance and assistance during sample pretreatment, and Lingling Xu and Mengren Li  
522 (Institute of Urban Environment, Chinese Academy of Sciences) for the discussion of  
523 this paper. This study was supported by Fujian Key Laboratory of Atmospheric Ozone  
524 Pollution Prevention and Xiamen Atmospheric Environment Observation and Research  
525 Station of Fujian Province (Institute of Urban Environment, Chinese Academy of  
526 Sciences).

527

528 **Financial support.** This research was financially supported by the Xiamen Youth  
529 Innovation Fund Project (3502Z20206094), the foreign cooperation project of Fujian  
530 Province (2020I0038), the Cultivating Project of Strategic Priority Research Program  
531 of Chinese Academy of Sciences (XDPB1903), the National Key Research and  
532 Development Program (2016YFC0112200), State Key Laboratory of Environmental  
533 Chemistry and Ecotoxicology, Research Center for Eco-Environmental Sciences, CAS  
534 (KF2020-06), the FJIRSM&IUE Joint Research Fund (RHZX-2019-006) and center for  
535 Excellence in Regional Atmospheric Environment project (E0L1B20201).

536

## 537 **Reference**

- 538 Charan, S. M., Huang, Y., and Seinfeld, J. H.: Computational Simulation of Secondary  
539 Organic Aerosol Formation in Laboratory Chambers, *Chem. Rev.*, 119, 11912-11944,  
540 10.1021/acs.chemrev.9b00358, 2019.
- 541 Cheng, Y., Ma, Y., and Hu, D.: Tracer-based source apportioning of atmospheric organic  
542 carbon and the influence of anthropogenic emissions on secondary organic aerosol  
543 formation in Hong Kong, *Atmos. Chem. Phys.*, 21, 10589-10608, 10.5194/acp-21-  
544 10589-2021, 2021.
- 545 Dhulipala, S. V., Bhandari, S., and Hildebrandt Ruiz, L.: Formation of oxidized organic  
546 compounds from Cl-initiated oxidation of toluene, *Atmospheric Environment*, 199, 265-  
547 273, 10.1016/j.atmosenv.2018.11.002, 2019.
- 548 Ding, X., He, Q.-F., Shen, R.-Q., Yu, Q.-Q., and Wang, X.-M.: Spatial distributions of  
549 secondary organic aerosols from isoprene, monoterpenes, beta-caryophyllene, and  
550 aromatics over China during summer, *Journal of Geophysical Research-Atmospheres*,  
551 119, 11877-11891, 10.1002/2014jd021748, 2014.

552 Fountoukis, C., and Nenes, A.: ISORROPIA II: a computationally efficient  
553 thermodynamic equilibrium model for  $K^+Ca^{2+}Mg^{2+}NH_4^+Na^+SO_4^{2-}$  –  
554  $NO_3^-Cl^-H_2O$  aerosols, *Atmos. Chem. Phys.*, 7, 4639-4659, 10.5194/acp-7-  
555 4639-2007, 2007.

556 Fu, P., Kawamura, K., Chen, J., and Barrie, L. A.: Isoprene, Monoterpene, and Sesquiterpene  
557 Oxidation Products in the High Arctic Aerosols during Late Winter to Early Summer,  
558 *Environmental Science & Technology*, 43, 4022-4028, 10.1021/es803669a, 2009.

559 Guo, H., Sullivan, A. P., Campuzano-Jost, P., Schroder, J. C., Lopez-Hilfiker, F. D.,  
560 Dibb, J. E., Jimenez, J. L., Thornton, J. A., Brown, S. S., Nenes, A., and Weber,  
561 R. J.: Fine particle pH and the partitioning of nitric acid during winter in the  
562 northeastern United States, *Journal of Geophysical Research: Atmospheres*, 121,  
563 10,355-310,376, <https://doi.org/10.1002/2016JD025311>, 2016.

564 Guo, H., Weber, R. J., and Nenes, A.: High levels of ammonia do not raise fine particle pH  
565 sufficiently to yield nitrogen oxide-dominated sulfate production, *Scientific Reports*, 7,  
566 12109, 10.1038/s41598-017-11704-0, 2017.

567 Hallquist, M., Wenger, J. C., Baltensperger, U., Rudich, Y., Simpson, D., Claeys, M.,  
568 Dommen, J., Donahue, N. M., George, C., Goldstein, A. H., Hamilton, J. F., Herrmann,  
569 H., Hoffmann, T., Iinuma, Y., Jang, M., Jenkin, M. E., Jimenez, J. L., Kiendler-Scharr,  
570 A., Maenhaut, W., McFiggans, G., Mentel, T. F., Monod, A., Prevot, A. S. H., Seinfeld,  
571 J. H., Surratt, J. D., Szmigielski, R., and Wildt, J.: The formation, properties and impact  
572 of secondary organic aerosol: current and emerging issues, *Atmospheric Chemistry and  
573 Physics*, 9, 5155-5236, 10.5194/acp-9-5155-2009, 2009.

574 Hao, L., Kari, E., Leskinen, A., Worsnop, D. R., and Virtanen, A.: Direct contribution of  
575 ammonia to  $\alpha$ -pinene secondary organic aerosol formation, *Atmos. Chem. Phys.*, 20,  
576 14393-14405, 10.5194/acp-20-14393-2020, 2020.

577 Hoffmann, D., Tilgner, A., Iinuma, Y., and Herrmann, H.: Atmospheric Stability of  
578 Levoglucosan: A Detailed Laboratory and Modeling Study, *Environmental Science &  
579 Technology*, 44, 694-699, 10.1021/es902476f, 2010.

580 Hong, Y., Xu, X., Liao, D., Zheng, R., Ji, X., Chen, Y., Xu, L., Li, M., Wang, H., Xiao, H.,  
581 Choi, S.-D., and Chen, J.: Source apportionment of PM<sub>2.5</sub> and sulfate formation during  
582 the COVID-19 lockdown in a coastal city of southeast China, *Environmental Pollution*,  
583 286, 117577, <https://doi.org/10.1016/j.envpol.2021.117577>, 2021.

584 Hong, youwei. (2022). Dataset for ACP by Hong et al., 2022 [Data set]. Zenodo.  
585 <https://doi.org/10.5281/zenodo.6376025>

586 Hong, Z., Zhang, H., Zhang, Y., Xu, L., Liu, T., Xiao, H., Hong, Y., Chen, J., Li, M., Deng,  
587 J., Wu, X., Hu, B., and Chen, X.: Secondary organic aerosol of PM<sub>2.5</sub> in a mountainous  
588 forest area in southeastern China: Molecular compositions and tracers implication,  
589 *Science of the Total Environment*, 653, 496-503, 10.1016/j.scitotenv.2018.10.370, 2019.

590 Hoyle, C. R., Boy, M., Donahue, N. M., Fry, J. L., Glasius, M., Guenther, A., Hallar, A. G.,  
591 Hartz, K. H., Petters, M. D., Petaja, T., Rosenoern, T., and Sullivan, A. P.: A review of  
592 the anthropogenic influence on biogenic secondary organic aerosol, *Atmospheric  
593 Chemistry and Physics*, 11, 321-343, 10.5194/acp-11-321-2011, 2011.

594 Hu, B., Liu, T., Hong, Y., Xu, L., Li, M., Wu, X., Wang, H., Chen, J., and Chen, J.:  
595 Characteristics of peroxyacetyl nitrate (PAN) in a coastal city of southeastern China:  
596 Photochemical mechanism and pollution process, *Science of the Total Environment*,  
597 719, 10.1016/j.scitotenv.2020.137493, 2020.

598 Hu, W., Palm, B. B., Day, D. A., Campuzano-Jost, P., Krechmer, J. E., Peng, Z., de Sa, S. S.,  
599 Martin, S. T., Alexander, M. L., Baumann, K., Hacker, L., Kiendler-Scharr, A., Koss, A.  
600 R., de Gouw, J. A., Goldstein, A. H., Seco, R., Sjostedt, S. J., Park, J.-H., Guenther, A.  
601 B., Kim, S., Canonaco, F., Prevot, A. S. H., Brune, W. H., and Jimenez, J. L.: Volatility  
602 and lifetime against OH heterogeneous reaction of ambient isoprene-epoxydiols-derived

603 secondary organic aerosol (IEPOX-SOA), *Atmospheric Chemistry and Physics*, 16,  
604 11563-11580, 10.5194/acp-16-11563-2016, 2016.

605 Jaoui, M., Kleindienst, T. E., Lewandowski, M., Offenberg, J. H., and Edney, E. O.:  
606 Identification and quantification of aerosol polar oxygenated compounds bearing  
607 carboxylic or hydroxyl groups. 2. Organic tracer compounds from monoterpenes,  
608 *Environmental Science & Technology*, 39, 5661-5673, 10.1021/es048111b, 2005.

609 Jaoui, M., Lewandowski, M., Kleindienst, T. E., Offenberg, J. H., and Edney, E. O.:  $\beta$ -  
610 caryophyllinic acid: An atmospheric tracer for  $\beta$ -caryophyllene secondary organic  
611 aerosol, *Geophysical Research Letters*, 34, 10.1029/2006gl028827, 2007.

612 Kari, E., Hao, L. Q., Ylisirnio, A., Buchholz, A., Leskinen, A., Yli-Pirila, P., Nuutinen, I.,  
613 Kuusalo, K., Jokiniemi, J., Faiola, C. L., Schobesberger, S., and Virtanen, A.: Potential  
614 dual effect of anthropogenic emissions on the formation of biogenic secondary organic  
615 aerosol (BSOA), *Atmospheric Chemistry and Physics*, 19, 15651-15671, 10.5194/acp-  
616 19-15651-2019, 2019.

617 Kleindienst, T. E., Jaoui, M., Lewandowski, M., Offenberg, J. H., Lewis, C. W., Bhawe, P. V.,  
618 and Edney, E. O.: Estimates of the contributions of biogenic and anthropogenic  
619 hydrocarbons to secondary organic aerosol at a southeastern US location, *Atmospheric  
620 Environment*, 41, 8288-8300, 10.1016/j.atmosenv.2007.06.045, 2007.

621 Lewandowski, M., Piletic, I. R., Kleindienst, T. E., Offenberg, J. H., Beaver, M. R., Jaoui, M.,  
622 Docherty, K. S., and Edney, E. O.: Secondary organic aerosol characterisation at field  
623 sites across the United States during the spring-summer period, *International Journal of  
624 Environmental Analytical Chemistry*, 93, 1084-1103, 10.1080/03067319.2013.803545,  
625 2013.

626 Liu, S., Tsona, N. T., Zhang, Q., Jia, L., Xu, Y., and Du, L.: Influence of relative humidity on  
627 cyclohexene SOA formation from OH photooxidation, *Chemosphere*, 231, 478-486,  
628 10.1016/j.chemosphere.2019.05.131, 2019.

629 Liu, S., Huang, D., Wang, Y., Zhang, S., Wu, C., Du, W., and Wang, G.: Synergetic effect of  
630  $\text{NH}_3$  and  $\text{NO}_x$  on the production and optical absorption of secondary organic aerosol  
631 formation from toluene photooxidation, *Atmos. Chem. Phys. Discuss.*, 2021, 1-38,  
632 10.5194/acp-2021-560, 2021.

633 Liu, T., Hu, B., Xu, X., Hong, Y., Zhang, Y., Wu, X., Xu, L., Li, M., Chen, Y., Chen, X., and  
634 Chen, J.: Characteristics of  $\text{PM}_{2.5}$ -bound secondary organic aerosol tracers in a coastal  
635 city in Southeastern China: Seasonal patterns and pollution identification, *Atmospheric  
636 Environment*, 237, 10.1016/j.atmosenv.2020.117710, 2020.

637 Lopez-Hilfiker, F. D., Mohr, C., D'Ambro, E. L., Lutz, A., Riedel, T. P., Gaston, C. J., Iyer,  
638 S., Zhang, Z., Gold, A., Surratt, J. D., Lee, B. H., Kurten, T., Hu, W. W., Jimenez, J.,  
639 Hallquist, M., and Thornton, J. A.: Molecular Composition and Volatility of Organic  
640 Aerosol in the Southeastern US: Implications for IEPDX Derived SOA, *Environmental  
641 Science & Technology*, 50, 2200-2209, 10.1021/acs.est.5b04769, 2016.

642 Lowes, S., Jersey, J., Shoup, R., Garofolo, F., Savoie, N., Mortz, E., Needham, S., Caturla, M.  
643 C., Steffen, R., Sheldon, C., Hayes, R., Samuels, T., Di Donato, L., Kamerud, J.,  
644 Michael, S., Lin, Z. P., Hillier, J., Moussallie, M., Teixeira, L. D., Rocci, M., Buonarati,  
645 M., Truong, J., Hussain, S., Lundberg, R., Breau, A., Zhang, T. Y., Jonker, J., Berger, N.,  
646 Gagnon-Carignan, S., Nehls, C., Nicholson, R., Hilhorst, M., Karnik, S., de Boer, T.,  
647 Houghton, R., Smith, K., Cojocar, L., Allen, M., Harter, T., Fatmi, S., Sayyarpour, F.,  
648 Vija, J., Malone, M., and Heller, D.: Recommendations on: internal standard criteria,  
649 stability, incurred sample reanalysis and recent 483s by the Global CRO Council for  
650 Bioanalysis, *Bioanalysis*, 3, 1323-1332, 10.4155/Bio.11.135, 2011.

651 Luo, H., Jia, L., Wan, Q., An, T., and Wang, Y.: Role of liquid water in the formation of O-3  
652 and SOA particles from 1,2,3-trimethylbenzene, *Atmospheric Environment*, 217,  
653 10.1016/j.atmosenv.2019.116955, 2019.

654 Lv, S., Wang, F., Wu, C., Chen, Y., Liu, S., Zhang, S., Li, D., Du, W., Zhang, F., Wang, H.,  
655 Huang, C., Fu, Q., Duan, Y., and Wang, G.: Gas-to-Aerosol Phase Partitioning of



656 Atmospheric Water-Soluble Organic Compounds at a Rural Site in China: An Enhancing  
657 Effect of NH<sub>3</sub> on SOA Formation, *Environmental Science & Technology*,  
658 10.1021/acs.est.1c06855, 2022.

659 Ma, Q., Lin, X. X., Yang, C. G., Long, B., Gai, Y. B., and Zhang, W. J.: The influences of  
660 ammonia on aerosol formation in the ozonolysis of styrene: roles of Criegee intermediate  
661 reactions, *Roy Soc Open Sci*, 5, ARTN 17217110.1098/rsos.172171, 2018.

662 Mahilang, M., Deb, M. K., and Pervez, S.: Biogenic secondary organic aerosols: A review on  
663 formation mechanism, analytical challenges and environmental impacts, *Chemosphere*,  
664 262, 10.1016/j.chemosphere.2020.127771, 2021.

665 McFiggans, G., Mentel, T. F., Wildt, J., Pullinen, I., Kang, S., Kleist, E., Schmitt, S.,  
666 Springer, M., Tillmann, R., Wu, C., Zhao, D. F., Hallquist, M., Faxon, C., Le Breton, M.,  
667 Hallquist, A. M., Simpson, D., Bergstrom, R., Jenkin, M. E., Ehn, M., Thornton, J. A.,  
668 Alfarra, M. R., Bannan, T. J., Percival, C. J., Priestley, M., Topping, D., and Kiendler-  
669 Scharr, A.: Secondary organic aerosol reduced by mixture of atmospheric vapours,  
670 *Nature*, 565, 587-593, 10.1038/s41586-018-0871-y, 2019.

671 Na, K., Song, C., Switzer, C., and Cocker, D. R.: Effect of Ammonia on Secondary Organic  
672 Aerosol Formation from  $\alpha$ -Pinene Ozonolysis in Dry and Humid Conditions,  
673 *Environmental Science & Technology*, 41, 6096-6102, 10.1021/es061956y, 2007.

674 Newland, M. J., Bryant, D. J., Dunmore, R. E., Bannan, T. J., Acton, W. J. F., Langford, B.,  
675 Hopkins, J. R., Squires, F. A., Dixon, W., Drysdale, W. S., Ivatt, P. D., Evans, M. J.,  
676 Edwards, P. M., Whalley, L. K., Heard, D. E., Slater, E. J., Woodward-Massey, R., Ye,  
677 C., Mehra, A., Worrall, S. D., Bacak, A., Coe, H., Percival, C. J., Hewitt, C. N., Lee, J.  
678 D., Cui, T., Surratt, J. D., Wang, X., Lewis, A. C., Rickard, A. R., and Hamilton, J. F.:  
679 Low-NO atmospheric oxidation pathways in a polluted megacity, *Atmos. Chem. Phys.*,  
680 21, 1613-1625, 10.5194/acp-21-1613-2021, 2021.

681 Offenberg, J. H., Lewis, C. W., Lewandowski, M., Jaoui, M., Kleindienst, T. E., and Edney,  
682 E. O.: Contributions of toluene and alpha-pinene to SOA formed in an irradiated  
683 toluene/alpha-pinene/NO<sub>x</sub>/air mixture: Comparison of results using C-14 content and  
684 SOA organic tracer methods, *Environmental Science & Technology*, 41, 3972-3976,  
685 10.1021/es070089+, 2007.

686 Offenberg, J. H., Lewandowski, M., Edney, E. O., Kleindienst, T. E., and Jaoui, M.: Influence  
687 of Aerosol Acidity on the Formation of Secondary Organic Aerosol from Biogenic  
688 Precursor Hydrocarbons, *Environmental Science & Technology*, 43, 7742-7747,  
689 10.1021/es901538e, 2009.

690 Palmer, P. I., Marvin, M. R., Siddans, R., Kerridge, B. J., and Moore, D. P.: Nocturnal  
691 survival of isoprene linked to formation of upper tropospheric organic aerosol, *Science*,  
692 375, 562-566, doi:10.1126/science.abg4506, 2022.

693 Reid, J. P., Bertram, A. K., Topping, D. O., Laskin, A., Martin, S. T., Petters, M. D., Pope, F.  
694 D., and Rovelli, G.: The viscosity of atmospherically relevant organic particles, *Nature*  
695 *Communications*, 9, 10.1038/s41467-018-03027-z, 2018.

696 Riva, M., Budisulistiorini, S. H., Zhang, Z., Gold, A., and Surratt, J. D.: Chemical  
697 characterization of secondary organic aerosol constituents from isoprene ozonolysis in  
698 the presence of acidic aerosol, *Atmospheric Environment*, 130, 5-13,  
699 10.1016/j.atmosenv.2015.06.027, 2016.

700 Rumsey, I. C., Cowen, K. A., Walker, J. T., Kelly, T. J., Hanft, E. A., Mishoe, K.,  
701 Rogers, C., Proost, R., Beachley, G. M., Lear, G., Frelink, T., and Otjes, R. P.:  
702 An assessment of the performance of the Monitor for AeRosols and Gases in  
703 ambient air (MARGA): a semi-continuous method for soluble compounds,  
704 *Atmos. Chem. Phys.*, 14, 5639-5658, 10.5194/acp-14-5639-2014, 2014.

705 Sarrafzadeh, M., Wildt, J., Pullinen, I., Springer, M., Kleist, E., Tillmann, R., Schmitt, S. H.,  
706 Wu, C., Mentel, T. F., Zhao, D., Hastie, D. R., and Kiendler-Scharr, A.: Impact of NO<sub>x</sub>  
707 and OH on secondary organic aerosol formation from beta-pinene photooxidation,

708 Atmospheric Chemistry and Physics, 16, 11237-11248, 10.5194/acp-16-11237-2016,  
709 2016.

710 Shrivastava, M., Cappa, C. D., Fan, J., Goldstein, A. H., Guenther, A. B., Jimenez, J. L.,  
711 Kuang, C., Laskin, A., Martin, S. T., Ng, N. L., Petaja, T., Pierce, J. R., Rasch, P. J.,  
712 Roldin, P., Seinfeld, J. H., Shilling, J., Smith, J. N., Thornton, J. A., Volkamer, R.,  
713 Wang, J., Worsnop, D. R., Zaveri, R. A., Zelenyuk, A., and Zhang, Q.: Recent advances  
714 in understanding secondary organic aerosol: Implications for global climate forcing,  
715 *Reviews of Geophysics*, 55, 509-559, 10.1002/2016rg000540, 2017.

716 Shrivastava, M., Andreae, M. O., Artaxo, P., Barbosa, H. M. J., Berg, L. K., Brito, J., Ching,  
717 J., Easter, R. C., Fan, J., Fast, J. D., Feng, Z., Fuentes, J. D., Glasius, M., Goldstein, A.  
718 H., Alves, E. G., Gomes, H., Gu, D., Guenther, A., Jathar, S. H., Kim, S., Liu, Y., Lou,  
719 S., Martin, S. T., McNeill, V. F., Medeiros, A., de Sa, S. S., Shilling, J. E., Springston, S.  
720 R., Souza, R. A. F., Thornton, J. A., Isaacman-VanWertz, G., Yee, L. D., Ynoue, R.,  
721 Zaveri, R. A., Zelenyuk, A., and Zhao, C.: Urban pollution greatly enhances formation of  
722 natural aerosols over the Amazon rainforest, *Nature Communications*, 10,  
723 10.1038/s41467-019-08909-4, 2019.

724 Song, M., Zhang, C., Wu, H., Mu, Y., Ma, Z., Zhang, Y., Liu, J., and Li, X.: The influence of  
725 OH concentration on SOA formation from isoprene photooxidation, *Science of the Total  
726 Environment*, 650, 951-957, 10.1016/j.scitotenv.2018.09.084, 2019.

727 Surratt, J. D., Lewandowski, M., Offenberg, J. H., Jaoui, M., Kleindienst, T. E., Edney, E. O.,  
728 and Seinfeld, J. H.: Effect of acidity on secondary organic aerosol formation from  
729 isoprene, *Environmental Science & Technology*, 41, 5363-5369, 10.1021/es0704176,  
730 2007.

731 Surratt, J. D., Chan, A. W. H., Eddingsaas, N. C., Chan, M., Loza, C. L., Kwan, A. J., Hersey,  
732 S. P., Flagan, R. C., Wennberg, P. O., and Seinfeld, J. H.: Reactive intermediates  
733 revealed in secondary organic aerosol formation from isoprene, *Proceedings of the  
734 National Academy of Sciences of the United States of America*, 107, 6640-6645,  
735 10.1073/pnas.0911114107, 2010.

736 Wang, D. S., and Ruiz, L. H.: Secondary organic aerosol from chlorine-initiated oxidation of  
737 isoprene, *Atmos. Chem. Phys.*, 17, 13491-13508, 10.5194/acp-17-13491-2017, 2017.

738 Wang, J., Ye, J., Zhang, Q., Zhao, J., Wu, Y., Li, J., Liu, D., Li, W., Zhang, Y., Wu, C., Xie,  
739 C., Qin, Y., Lei, Y., Huang, X., Guo, J., Liu, P., Fu, P., Li, Y., Lee, H. C., Choi, H.,  
740 Zhang, J., Liao, H., Chen, M., Sun, Y., Ge, X., Martin, S. T., and Jacob, D. J.: Aqueous  
741 production of secondary organic aerosol from fossil-fuel emissions in winter Beijing  
742 haze, *Proc Natl Acad Sci U S A*, 118, 10.1073/pnas.2022179118, 2021a.

743 Wang, J., Ye, J., Zhang, Q., Zhao, J., Wu, Y., Li, J., Liu, D., Li, W., Zhang, Y., Wu, C., Xie,  
744 C., Qin, Y., Lei, Y., Huang, X., Guo, J., Liu, P., Fu, P., Li, Y., Lee, H. C., Choi, H.,  
745 Zhang, J., Liao, H., Chen, M., Sun, Y., Ge, X., Martin, S. T., and Jacob, D. J.: Aqueous  
746 production of secondary organic aerosol from fossil-fuel emissions in winter Beijing  
747 haze, *Proceedings of the National Academy of Sciences of the United States of America*,  
748 118, 10.1073/pnas.2022179118, 2021b.

749 Wang, S., Du, L., Tsona, N. T., Jiang, X., You, B., Xu, L., Yang, Z., and Wang, W.: Effect of  
750 NO<sub>x</sub> and SO<sub>2</sub> on the photooxidation of methylglyoxal: Implications in secondary  
751 aerosol formation, *J Environ Sci (China)*, 92, 151-162, 10.1016/j.jes.2020.02.011, 2020.

752 Wang, X., Jacob, D. J., Downs, W., Zhai, S., Zhu, L., Shah, V., Holmes, C. D., Sherwen, T.,  
753 Alexander, B., Evans, M. J., Eastham, S. D., Neuman, J. A., Veres, P. R., Koenig, T. K.,  
754 Volkamer, R., Huey, L. G., Bannan, T. J., Percival, C. J., Lee, B. H., and Thornton, J. A.:  
755 Global tropospheric halogen (Cl, Br, I) chemistry and its impact on oxidants, *Atmos.  
756 Chem. Phys.*, 21, 13973-13996, 10.5194/acp-21-13973-2021, 2021c.

757 Wen, L., Chen, T., Zheng, P., Wu, L., Wang, X., Mellouki, A., Xue, L., and Wang, W.:  
758 Nitrous acid in marine boundary layer over eastern Bohai Sea, China: Characteristics,  
759 sources, and implications, *Sci. Total Environ.*, 10.1016/j.scitotenv.2019.03.225, 2019.

760 Wu, X., Xu, L. L., Hong, Y. W., Chen, J. F., Qiu, Y. Q., Hu, B. Y., Hong, Z. Y., Zhang, Y.  
761 R., Liu, T. T., Chen, Y. T., Bian, Y. H., Zhao, G. Q., Chen, J. S., and Li, M. R.: The air  
762 pollution governed by subtropical high in a coastal city in Southeast China: Formation  
763 processes and influencing mechanisms, *Science of the Total Environment*, 692, 1135-  
764 1145, 10.1016/j.scitotenv.2019.07.341, 2019.

765 Wu, X., Li, M., Chen, J., Wang, H., Xu, L., Hong, Y., Zhao, G., Hu, B., Zhang, Y., Dan, Y.,  
766 and Yu, S.: The characteristics of air pollution induced by the quasi-stationary front:  
767 Formation processes and influencing factors, *Science of the Total Environment*, 707,  
768 10.1016/j.scitotenv.2019.136194, 2020.

769 Xiao, Y., Wu, Z., Guo, S., He, L., Huang, X., and Hu, M.: Formation mechanism of  
770 secondary organic aerosol in aerosol liquid water: A review, *Chinese Science Bulletin*,  
771 65, 3118-3133, 2020.

772 Xu, L., Du, L., Tsona, N. T., and Ge, M. F.: Anthropogenic Effects on Biogenic Secondary  
773 Organic Aerosol Formation, *Advances in Atmospheric Sciences*, 38, 1053-1084,  
774 10.1007/s00376-020-0284-3, 2021.

775 Xu, L., Guo, H. Y., Boyd, C. M., Klein, M., Bougiatioti, A., Cerully, K. M., Hite, J. R.,  
776 Isaacman-VanWertz, G., Kreisberg, N. M., Knote, C., Olson, K., Koss, A., Goldstein, A.  
777 H., Hering, S. V., de Gouw, J., Baumann, K., Lee, S. H., Nenes, A., Weber, R. J., and  
778 Ng, N. L.: Effects of anthropogenic emissions on aerosol formation from isoprene and  
779 monoterpenes in the southeastern United States, *Proceedings of the National Academy of*  
780 *Sciences of the United States of America*, 112, 37-42, 10.1073/pnas.1417609112, 2015.

781 Yang, W., Cao, J., Wu, Y., Kong, F., and Li, L.: Review on plant terpenoid emissions  
782 worldwide and in China, *The Science of the total environment*, 787, 147454-147454,  
783 10.1016/j.scitotenv.2021.147454, 2021.

784 Zhang, J., An, J., Qu, Y., Liu, X., and Chen, Y.: Impacts of potential HONO sources on the  
785 concentrations of oxidants and secondary organic aerosols in the Beijing-Tianjin-Hebei  
786 region of China, *Science of the Total Environment*, 647, 836-852,  
787 10.1016/j.scitotenv.2018.08.030, 2019a.

788 Zhang, P., Chen, T., Liu, J., Liu, C., Ma, J., Ma, Q., Chu, B., and He, H.: Impacts of SO<sub>2</sub>,  
789 Relative Humidity, and Seed Acidity on Secondary Organic Aerosol Formation in the  
790 Ozonolysis of Butyl Vinyl Ether, *Environmental Science & Technology*, 53, 8845-8853,  
791 10.1021/acs.est.9b02702, 2019b.

792 Zhang, Y.-Q., Chen, D.-H., Ding, X., Li, J., Zhang, T., Wang, J.-Q., Cheng, Q., Jiang, H.,  
793 Song, W., Ou, Y.-B., Ye, P.-L., Zhang, G., and Wang, X.-M.: Impact of anthropogenic  
794 emissions on biogenic secondary organic aerosol: observation in the Pearl River Delta,  
795 southern China, *Atmospheric Chemistry and Physics*, 19, 14403-14415, 10.5194/acp-19-  
796 14403-2019, 2019c.

797 Zhang, Y., Chen, Y., Lei, Z., Olson, N. E., Riva, M., Koss, A. R., Zhang, Z., Gold, A., Jayne,  
798 J. T., Worsnop, D. R., Onasch, T. B., Kroll, J. H., Turpin, B. J., Ault, A. P., and Surratt,  
799 J. D.: Joint Impacts of Acidity and Viscosity on the Formation of Secondary Organic  
800 Aerosol from Isoprene Epoxydiols (IEPDX) in Phase Separated Particles, *Acs Earth and*  
801 *Space Chemistry*, 3, 2646-2658, 10.1021/acsearthspacechem.9b00209, 2019d.

802 Zhao, D. F., Schmitt, S. H., Wang, M. J., Acir, I. H., Tillmann, R., Tan, Z. F., Novelli, A.,  
803 Fuchs, H., Pullinen, I., Wegener, R., Rohrer, F., Wildt, J., Kiendler-Scharr, A., Wahner,  
804 A., and Mentel, T. F.: Effects of NO<sub>x</sub> and SO<sub>2</sub> on the secondary organic aerosol  
805 formation from photooxidation of alpha-pinene and limonene, *Atmospheric Chemistry*  
806 *and Physics*, 18, 1611-1628, 10.5194/acp-18-1611-2018, 2018.

807 Zheng, G., Su, H., Wang, S., Andreae, M. O., Poschl, U., and Cheng, Y.: Multiphase buffer  
808 theory explains contrasts in atmospheric aerosol acidity, *Science*, 369, 1374-+,  
809 10.1126/science.aba3719, 2020.

810 Zhou, M., Zheng, G., Wang, H., Qiao, L., Zhu, S., Huang, D., An, J., Lou, S., Tao, S., Wang,  
811 Q., Yan, R., Ma, Y., Chen, C., Cheng, Y., Su, H., and Huang, C.: Long-term trends and

812 drivers of aerosol pH in eastern China, *Atmos. Chem. Phys. Discuss.*, 2021, 1-21,  
813 10.5194/acp-2021-455, 2021.  
814 Zhu, J., Penner, J. E., Yu, F., Sillman, S., Andreae, M. O., and Coe, H.: Decrease in radiative  
815 forcing by organic aerosol nucleation, climate, and land use change, *Nature*  
816 *Communications*, 10, 10.1038/s41467-019-08407-7, 2019.

817

818

819